UCLA
COMPUTATIONAL AND APPLIED MATHEMATICS

An Efficient Numerical Method for 3D Flow Around a Submerged Body

Johan F. Malmliden

February 1995

CAM Report 95-7

Department of Mathematics
University of California, Los Angeles
Los Angeles, CA. 90024-1555

An Efficient Numerical Method for 3D Flow around a Submerged Body

Johan F. Malmliden*
Center for Computational Mathematics and Mechanics
Royal Institute of Technology, Stockholm, Sweden

August 18, 1994

Abstract

In this paper we present an efficient Schwarz type iterative method for computing the steady linearized 3-D free surface potential flow around a submerged body, moving in a liquid of finite constant depth at constant speed and distance below the surface.

The 3-D problem is too large to be solved using a direct method. It is also indefinite, which makes the convergence of most iterative methods unstable. We therefore construct an iterative method by decomposing the original problem into two simpler subproblems. We then form a Schwarz type iteration between the subproblems. At convergence the solution to the original problem is given by the sum of the solutions to the subproblems.

The subproblems can be chosen so that they are mathematically simple and fast to solve. The convergence of this iterative method is fast. It is proven that the iterative method converges for sufficiently small Froude numbers.

We present a careful validation of this method. The implementation of the iterative method, described in this paper, is numerically shown to be second order accurate. The number of operations necessary for solving this problem is proportional to the work needed to solve a definite elliptic problem. If we use a Biconjugate gradient method the number of operations is proportional to $n^{4/3}$ and if we use a Multigrid method the number of operations is proportional to $n\log(n)$, where n is the number of unknowns in the discretized problem. The coefficient of drag computed with this method agrees well with that obtained by existing methods.

*Partially supported by ONR grant N-00014-90-J-1382, NSF grant DMS 90-61311 and by the U.S. Department of Energy through Los Alamos National Laboratory.

Contents

1 Introduction **3**

2 The Indefinite Subproblem **5**

3 Analysis of the Iteration **10**
3.1 Estimate for the Definite Subproblem 11
3.2 Estimates for the Indefinite Subproblem 11
3.3 Proof of Convergence of the Iterative Cycle. 15

4 Farfield Boundary Conditions **15**
4.1 Behaviour of the Solution to the Definite Problem ahead of and after the Submerged Body. 17

5 Numerical Method **19**
5.1 Solving the Definite Subproblem 19
5.2 Solving the Indefinite Subproblem 20

6 Numerical Results **20**
6.1 Numerical Testing and Validation 21

7 Conclusions **27**

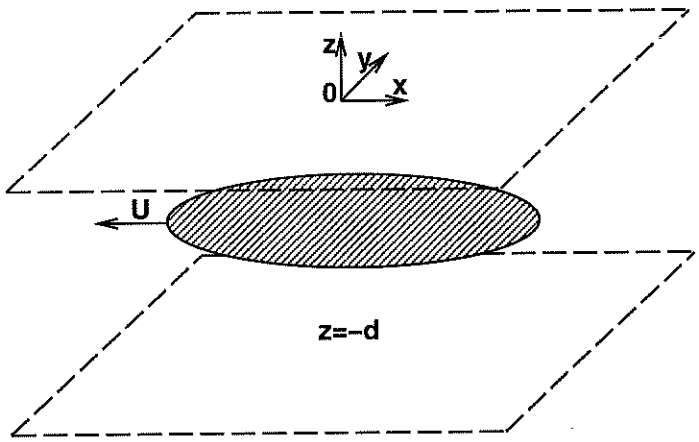

Figure 1: A submerged body travelling at constant speed and direction. The coordinate system is fixed with respect to the body.

1 Introduction

The subject of this paper is an efficient, Schwartz–type, iterative method for computing the steady linearized 3–D potential flow around a submerged body moving in a liquid of finite constant depth. Let the depth of the liquid be d, the speed of the body be U and the acceleration of gravity be g. After scaling the physical quantities by the length d and the velocity $\sqrt{gd}$, we get the problem depicted in figure 1.

The total velocity potential is split into the sum of a free stream potential and a perturbation potential; $\Phi(x,y,z) = \mu x + \phi(x,y,z)$, where $\mu = U/\sqrt{gd}$ is the Froude number and the x-axis lies in the direction of the farfield flow. The perturbation potential is governed by, cf. [11],

$$\Delta\phi = 0,\ -\infty < x < \infty,\ -\infty < y < \infty,\ -1 < z < 0, \tag{1}$$

together with the boundary conditions

$$\begin{aligned} \mu^2\phi_{xx} + \phi_z &= 0,\ -\infty < x < \infty,\ -\infty < y < \infty,\ z = 0, \\ \phi_z &= 0,\ -\infty < x < \infty,\ -\infty < y < \infty,\ z = -1, \\ \partial\phi/\partial n + \mu\cos\theta &= 0, \text{ on the body.} \end{aligned} \tag{2}$$

Here, $\partial/\partial n$ denotes the outward normal derivative and θ is the angle between the normal and the x-axis. We are looking for a solution where the perturbation potential tends to a constant value at large distances in front of the body. This condition is called the upstream condition,

$$\text{when } x \to -\infty \text{ then } \phi = C_1 + e^{C_2 x},\ -\infty < y < \infty,\ -1 < z < 0, \tag{3}$$

where C_2 is a positive constant and C_1 is an arbitrary constant. For simplicity, we choose to set $C_1 = 0$.

For the two-dimensional counterpart to the present problem, the most efficient solution approach is probably a direct method, cf. [10]. However, due to memory and work requirements, it is not possible to use a direct method to solve the three dimensional problem. The problem (1–3) is indefinite, which makes the convergence of most iterative methods unstable. To circumvent this difficulty, we decompose the problem into two more easily solvable subproblems and form a Schwarz–type iteration between these subproblems to solve the original problem.

The first subproblem, which will be refered to as the definite subproblem, is defined by

$$\Delta\phi^I = 0,\ -\infty < x < \infty,\ -\infty < y < \infty,\ -1 < z < 0, \tag{4}$$

together with the boundary conditions

$$\phi^I_z = 0,\ -\infty < x < \infty,\ -\infty < y < \infty,\ z = 0, \tag{5}$$
$$\phi^I_z = 0,\ -\infty < x < \infty,\ -\infty < y < \infty,\ z = -1, \tag{6}$$
$$\partial\phi^I/\partial n = h, \text{ on the body.} \tag{7}$$

To fix the undetermined constant in this Neumann problem we enforce

$$\text{when } x \to -\infty \text{ then } \phi^I = C_1 + e^{C_2 x},\ -\infty < y < \infty,\ -1 < z < 0, \tag{8}$$

where C_1 and C_2 are constants analogous to those in (3)

The second subproblem, which will be called the indefinite subproblem, does not have a submerged body in the interior of the domain. It is governed by,

$$\Delta\phi^{II} = 0,\ -\infty < x < \infty,\ -\infty < y < \infty,\ -1 < z < 0, \tag{9}$$

subject to the boundary conditions

$$\mu^2\phi^{II}_{xx} + \phi^{II}_z = t,\ -\infty < x < \infty,\ -\infty < y < \infty,\ z = 0, \tag{10}$$
$$\phi^{II}_z = 0,\ -\infty < x < \infty,\ -\infty < y < \infty,\ z = -1, \tag{11}$$

In order to make the solution unique, we enforce the upstream condition,

$$\text{when } x \to -\infty \text{ then } \phi^{II} = C_1 + e^{C_2 x},\ -\infty < y < \infty,\ -1 < z < 0, \tag{12}$$

The first subproblem is definite and can therefore be solved by standard iterative methods, for details see §5.1. The second subproblem is indefinite but has no body. It is therefore easily and efficiently solvable by separation of variables. This solution method is described in detail in §2 and §5.2.

The solutions of the subproblems are well defined once the forcing functions h and t are determined. It is clear that $\phi^I + \phi^{II}$ will solve (1–3) if we can find functions t and h that simultaneously satisfy $t(x,y) = -\mu^2\phi^I_{xx}(x,y,0)$ and

$h(x_b, y_b, z_b) = -\mu \cos\theta(x_b, y_b, z_b) - \partial\phi^{II}/\partial n(x_b, y_b, z_b)$, where the boundary of the body is described by $x_b = x_b(s,u)$, $y_b = y_b(s,u)$, $z_b = z_b(s,u)$, $0 \le s \le 1, 0 \le u \le 1$.
We compute h and t by iteration. The initial guess is taken to be $\phi^{II(0)}(x,y,z) \equiv 0$, then we iterate according to

1. Set $h^{(i)}(x_b, y_b, z_b) = -\mu \cos\theta(x_b, y_b, z_b) - \partial\phi^{II(i-1)}/\partial n(x_b, y_b, z_b)$ and solve the definite subproblem for $\phi^{I(i)}$.

2. Set $t^{(i)}(x,y) = -\mu^2 \phi_{xx}^{I(i)}(x,y,0)$, and solve the indefinite subproblem for $\phi^{II(i)}$.

The main result of this paper, which is proven in §3, is that the iteration converges for sufficiently small Froude numbers. In §4 to demonstrate the convergence numerically, we truncate the infinite domain in the x- and the y-direction and introduce farfield boundary conditions to carry out the practical computation. Finally in §5 we present numerical results for a second order accurate discretization of (1–3). We show that the iterative method converges rapidly, and that the convergence rate improves when the Froude number decreases. We also verify numerically that the convergence rate is essentially independent of the grid size.

2 The Indefinite Subproblem

To get a discrete Fourier spectrum we introduce side walls at $y = \pm a$ where the width a is a bounded constant. Here we impose the boundary condition $\phi_y^{II} = 0$. This corresponds to studying flow in a canal. We Fourier expand the indefinite subproblem (9-12) in the y-direction:

$$\phi^{II}(x,y,z) = \sum_{k=0}^{\infty} \hat{\phi}^{II}(x, \omega_y^{(k)}, z) \cdot \cos(\omega_y^{(k)} y), \tag{13}$$

where $\omega_y^{(k)} = k\pi/2a$, $k = 0, 1, 2, \ldots$. The expansion of the forcing t at the surface is:

$$t(x,y) = \sum_{k=0}^{\infty} \hat{t}(x, \omega_y^{(k)}) \cdot \cos(\omega_y^{(k)} y) \tag{14}$$

By projection of the Fourier modes we have:

$$\hat{t}(x, \omega_y^{(k)}) = \frac{1}{2\pi} \int_{-\infty}^{\infty} t(x,y) \cdot \cos(\omega_y^{(k)} y) dy \Big/ \int_{-\infty}^{\infty} \cos^2(\omega_y^{(k)} y) dy. \tag{15}$$

We thus have the following equation system for $\hat{\phi}^{II}$ in Fourier space, skipping the hats.

$$\phi_{xx}^{II} - \omega_y^{(k)2} \phi^{II} + \phi_{zz}^{II} = 0, \; -\infty < x < \infty, \; -1 < z < 0, \tag{16}$$

and boundary conditions

$$\mu^2\phi^{II}_{xx} + \phi^{II}_z = t,\ -\infty < x < \infty,\ z = 0, \tag{17}$$
$$\phi^{II}_z = 0,\ -\infty < x < \infty,\ z = -1. \tag{18}$$

Henceforth, we assume that (16) is satisfied on the boundary $z = 0$ and enter the substitution $\phi^{II}_{xx} = \omega_y^{(k)2}\phi^{II} - \phi^{II}_{zz}$ in (17). We then split the solution according to: $\phi^{II} = \phi^a + \phi^s$. The idea is to use ϕ^a to move the inhomogenity from the surface boundary condition to an inhomogenity for the Laplace's equation and then solve the resulting problem for ϕ^s by separation of variables. The auxiliary function ϕ^a must satisfy

$$\begin{aligned}\mu^2(\omega_y^{(k)2}\phi^a - \phi^a_{zz}) + \phi^a_z = t,\ -\infty < x < \infty,\ z = 0,\\ \phi^a_z = 0,\ -\infty < x < \infty,\ z = -1.\end{aligned} \tag{19}$$

In the interior, ϕ^a is only required to be smooth. We will use the following simple solution:

$$\phi^a(x, \omega_y^{(k)}, z) = \frac{t(x, \omega_y^{(k)})}{(2 + \mu^2(\omega_y^{(k)2} - 2))}(1 + z)^2. \tag{20}$$

In order to make $\phi^a + \phi^s$ satisfy (16–18), ϕ^s has to fulfill

$$\phi^s_{xx} - \omega_y^{(k)2}\phi^s + \phi^s_{zz} = f(x, \omega_y^{(k)}, z),\ -\infty < x < \infty,\ -1 < z < 0,, \tag{21}$$

together with the boundary conditions

$$\begin{aligned}\mu^2(\omega_y^{(k)2}\phi^s - \phi^s_{zz}) + \phi^s_z = 0,\ -\infty < x < \infty,\ z = 0,\\ \phi^s_z = 0,\ -\infty < x < \infty,\ z = -1.\end{aligned} \tag{22}$$

where the forcing f is defined by

$$f = -\phi^a_{xx} + \omega_y^{(k)2}\phi^a - \phi^a_{zz} \tag{23}$$

To separate the x- and z-variables, we make the ansatz

$$\phi^s(x, \omega_y^{(k)}, z) = R(x, \omega_y^{(k)}) \cdot S(\omega_y^{(k)}, z). \tag{24}$$

Upon inserting this ansatz into (21), we have

$$(R_{xx} - \omega_y^{(k)2}R) \cdot S + R \cdot S_{zz} = 0, \rightarrow \tag{25}$$

$$\frac{S_{zz}}{S} = -\frac{R_{xx} - \omega_y^{(k)2}R}{R} = \omega_z^{(k,j)2}. \tag{26}$$

The equation system for $S(z)$ is:

$$S_{zz} - \omega_z^{(k,j)2}S = 0. \tag{27}$$

and the boundary conditions, obtained by inserting (24) into (22), are:

$$\mu^2(\omega_y^{(k)2}S - S_{zz}) + S_z = 0,\ z = 0, \tag{28}$$
$$S_z = 0,\ z = -1. \tag{29}$$

The z-eigenfunctions are given by:

$$\begin{aligned} &S^{(0)}(\omega_y^{(k)}, z) = 1, \text{ if } \omega_y^{(k)} = 0, \text{ otherwise } S^{(0)} = 0, \\ &S^{(1)}(\omega_y^{(k)}, z) = \cosh(\omega_z^{(k,1)}(1+z)), \\ &S^{(j)}(\omega_y^{(k)}, z) = \cos(\sigma_z^{(k,j)}(1+z)),\ j = 2,3,4,\ldots. \end{aligned} \tag{30}$$

Expressions for the eigenvalues $\omega_z^{(k,j)}$ are obtained by entering (24) and the corresponding eigenfunctions from (30) into the surface boundary condition (29):

$$\sinh(\omega_z^{(k,j)}) = \mu^2(\omega_z^{(k,j)} - \frac{\omega_y^{(k)2}}{\omega_z^{(k,j)}})\cosh(\omega_z^{(k,j)}),\ j = 1,2,3\ldots, \tag{31}$$

note that this equation simplify when $\omega_y^{(k)} = 0$.

If we assume that $0 < \mu < 1$ this equation has only one positive, real root $\omega_z^{(k,1)}$ and an infinite number of imaginary roots $\omega_z^{(k,j)} = i\sigma_z^{(k,j)}$, $j = 2,3,4,\ldots$. When $\mu \to 0$ we have:

$$\omega_z^{(k,1)} \to \frac{1}{2\mu^2} + \sqrt{\frac{1}{4\mu^4} + \omega_y^{(k)2}}.$$

The equation for the imaginary eigenvalues, $\sigma_z^{(k,j)}$ is:

$$\sin(\sigma_z^{(k,j)}) = \mu^2(\sigma_z^{(k,j)} + \frac{\omega_y^{(k)2}}{\sigma_z^{(k,j)}})\cos(\sigma_z^{(k,j)}),\ j = 2,3,4\ldots, \tag{32}$$

studying (32) gives the following bounds for $\sigma_z^{(k,j)}$, for $\omega_y^{(k)} = 0$:

$$j \cdot \pi < |\sigma_z^{(k,j)}| < (j + \frac{1}{2}) \cdot \pi,\ j = 2,3,4,\ldots, \tag{33}$$

and for $\omega_y^{(k)} \neq 0$:

$$(j-1) \cdot \pi < |\sigma_z^{(k,j)}| < (j - \frac{1}{2}) \cdot \pi,\ j = 2,3,4,\ldots. \tag{34}$$

The functions $\cosh z$ and $\cos z$ are symmetric in z; we will therefore only consider positive $\omega_z^{(k,1)}$ and $\sigma_z^{(k,j)}$.

We expand ϕ^s in the eigenfunctions $S^{(j)}(\omega_y^{(k)}, z)$:

$$\phi^s(x, \omega_y^{(k)}, z) = \sum_{j=0}^{\infty} R^{(j)}(x, \omega_y^{(k)}) \cdot S^{(j)}(\omega_y^{(k)}, z). \tag{35}$$

We also expand the the right hand side:

$$f(x,\omega_y^{(k)},z)=\sum_{j=0}^{\infty} f^{(j)}(x,\omega_y^{(k)})\cdot S^{(j)}(\omega_y^{(k)},z), \tag{36}$$

This is generally not a self adjoint problem. The eigenfunctions $S^{(j)}(\omega_y^{(k)},z)$ are not orthogonal in z. Therefore it is hard to compute $f^{(j)}$ and $R^{(j)}$ from this form of the equations. However it is shown in [9] that we can transform this problem to self adjoint form , by applying the following transformation to ϕ^s, where we use $\xi=1+z$ to clarify the notation. The self adjoint (transformed) problem has eigenfunctions that are orthogonal in z. Therefore we can use projection to calculate the coefficients: $f^{(j)}$ and $R^{(j)}$.

$$\tilde{\phi}^s(x,\omega_y^{(k)},\xi) = \frac{\cos(\beta^{(k,j)}\,\xi)}{\beta^{(k,j)}}\frac{d}{d\xi}\left(\frac{\phi^s(x,\omega_y^{(k)},\xi)}{\cos(\beta^{(k,j)}\,\xi)}\right), \tag{37}$$

$$\tilde{\phi}^s(x,\omega_y^{(k)},\xi) = \frac{\cosh(\alpha^{(k,j)}\,\xi)}{\alpha^{(k,j)}}\frac{d}{d\xi}\left(\frac{\phi^s(x,\omega_y^{(k)},\xi)}{\cosh(\alpha^{(k,j)}\,\xi)}\right). \tag{38}$$

where the $\alpha^{(k,j)}$ and $\beta^{(k,j)}$'s are given by the relations:

$$\begin{aligned}\tanh\alpha^{(k,j)} &= \mu^2\left(\alpha^{(k,j)}-\tfrac{\omega_y^{(k)2}}{\alpha^{(k,j)}}\right),\\ \tan\beta^{(k,j)} &= \mu^2\left(\beta^{(k,j)}+\tfrac{\omega_y^{(k)2}}{\beta^{(k,j)}}\right).\end{aligned} \tag{39}$$

To get a nonsingular transformation we must have $\beta^{(k,j)}<\pi/2$, for $k>0$ this is only satisfied for $j=1$. For $k=0$ there are two eigenvalues that we could use for a transformation: $\alpha^{(0,0)}>0$ and $\beta^{(0,1)}=0$. This yields $\alpha^{(0,0)}=\beta^{(0,0)}=0$, which gives $\cos(\beta^{(0,0)}\,\xi),\cosh(\alpha^{(0,0)}\,\xi)\equiv 1$. The simpler transformation d/dz is utilized in this case. If we enter (35,36) into (21) we arrive at the following system of ordinary differential equations in x:

$$\frac{d^2R^{(0)}}{dx^2} = f^{(0)}(x,\omega_y^{(k)}), \tag{40}$$

$$\frac{d^2R^{(1)}}{dx^2}+(\omega_z^{(k,1)2}-\omega_y^{(k)2})R^{(1)} = f^{(1)}(x,\omega_y^{(k)}), \tag{41}$$

$$\frac{d^2R^{(j)}}{dx^2}-(\sigma_z^{(k,j)2}+\omega_y^{(k)2})R^{(j)} = f^{(j)}(x,\omega_y^{(k)}),\ j=2,3,4,\ldots. \tag{42}$$

From (12,30) it is clear that $R^{(0)}=0$ for $\omega_y^{(k)}\neq 0$.

We define the inner product and norm in the z-direction,

$$\langle a,b\rangle_z=\int_{-1}^{0}\bar{a}b\,dz,\ \ \|a\|_z^2=\langle a,a\rangle_z. \tag{43}$$

We denote the transformed eigenfunctions $\zeta^{(j)}$:

$$\zeta^{(1)}(\omega_y^{(k)}, z) = \frac{\cos(\beta^{(k,1)}\,\xi)}{\beta^{(k,1)}} \frac{d}{d\xi}\left(\frac{S^{(1)}(\omega_y^{(k)}, \xi)}{\cos(\beta^{(k,1)}\,\xi)}\right), \tag{44}$$

$$\zeta^{(j)}(\omega_y^{(k)}, \xi) = \frac{\cosh(\alpha^{(k,0)}\,\xi)}{\alpha^{(k,0)}} \frac{d}{d\xi}\left(\frac{S^{(j)}(\omega_y^{(k)}, \xi)}{\cosh(\alpha^{(k,0)}\,\xi)}\right), j = 2, 3, 4, \ldots. \tag{45}$$

For simplicity, the transformed eigenfunctions are normalized:

$$\tilde{\zeta}^{(j)}(\omega_y^{(k)}, \xi) = \frac{\zeta^{(j)}}{||\zeta^{(j)}||_z},\ j = 1, 2, 3, \ldots, \tag{46}$$

It is shown in [9] that $\langle \zeta^{(j)}, \zeta^{(l)} \rangle_z = 0$ if $j \neq l$. We now develop the expressions (44,45) further by inserting (30)

$$\tilde{\zeta}^{(1)} = \frac{\omega_z^{(k,1)} \sinh(\omega_z^{(k,1)}\xi)\cos(\beta^{(k,1)}\,\xi) + \beta^{(k,1)}\cosh(\omega_z^{(k,1)}\xi)\sin(\beta^{(k,1)}\xi)}{\beta^{(k,1)}\cos(\beta^{(k,1)}\,\xi)||\zeta^{(1)}||_z}, \tag{47}$$

$$\tilde{\zeta}^{(j)} = -\frac{\sigma_z^{(k,j)} \sin(\sigma_z^{(k,j)}\xi)\cosh(\alpha^{(k,0)}\,\xi) + \alpha^{(k,0)}\cos(\sigma_z^{(k,j)}\xi)\sinh(\alpha^{(k,0)}\,\xi)}{\alpha^{(k,0)}\cosh(\alpha^{(k,0)}\,\xi)||\zeta^{(j)}||_z}, \tag{48}$$

for $j = 2, 3, 4, \ldots$.

We denote the transformed forcing $v(x, \omega_y^{(k)}, \xi)$:

$$v(x, \omega_y^{(k)}, \xi) = \frac{\cos(\beta^{(k,1)}\,\xi)}{\beta^{(k,1)}} \frac{d}{d\xi}\left(\frac{f(x, \omega_y^{(k)}, \xi)}{\cos(\beta^{(k,1)}\,\xi)}\right), \tag{49}$$

$$v(x, \omega_y^{(k)}, \xi) = \frac{\cosh(\alpha^{(k,0)}\,\xi)}{\alpha^{(k,0)}} \frac{d}{d\xi}\left(\frac{f(x, \omega_y^{(k)}, \xi)}{\cosh(\alpha^{(k,0)}\,\xi)}\right). \tag{50}$$

The transformed forcing $v(x, \omega_y^{(k)}, \xi)$ can now be written in terms of $f(x, \omega_y^{(k)}, \xi)$ and $f_\xi(x, \omega_y^{(k)}, \xi)$.

$$v(x, \omega_y^{(k)}, \xi) = \frac{f_\xi(x, \omega_y^{(k)}, \xi)\cos(\beta^{(k,1)}\,\xi) + \beta^{(k,1)} f(x, \omega_y^{(k)}, \xi)\sin(\beta^{(k,1)}\,\xi)}{\beta^{(k,1)}\cos(\beta^{(k,1)}\,\xi)}, \tag{51}$$

$$v(x, \omega_y^{(k)}, \xi) = \frac{f_\xi(x, \omega_y^{(k)}, \xi)\cosh(\alpha^{(k,0)}\,\xi) - \alpha^{(k,0)} f(x, \omega_y^{(k)}, \xi)\sinh(\alpha^{(k,0)}\,\xi)}{\alpha^{(k,0)}\cosh(\alpha^{(k,0)}\,\xi)}. \tag{52}$$

Each mode $f^{(j)}(x, \omega_y^{(k)})$ can be computed by transforming (36) as indicated in (44) and entering (49,50). We then project $f^{(j)}(x, \omega_y^{(k)})$ by using the orthogonality of the transformed eigenfunctions wrt. the z-inner product.

$$f^{(j)} = \frac{\langle v, \tilde{\zeta}^{(j)} \rangle_z}{||\tilde{\zeta}^{(j)}||_z^2} = \langle v, \tilde{\zeta}^{(j)} \rangle_z,\ j = 1, 2, 3, \ldots. \tag{53}$$

For the case when $\omega_y^{(0)} = 0$, the expressions for $f^{(j)}$, $j = 0, 1, 2, \ldots$ simplify considerably and it is possible to evaluate them analytically. We have:

$$f^{(1)}(x) = \frac{-4t''(x,\omega_y^{(0)})}{1-\mu^2} \cdot \frac{\sinh\omega_z^{(0,1)} - \omega_z^{(0,1)}\cosh\omega_z^{(0,1)}}{2\omega_z^{(0,1)3} - \omega_z^{(0,1)2}\sinh 2\omega_z^{(0,1)}} =$$

$$= \frac{2t''\cosh\omega_z^{(0,1)}}{\omega_z^{(0,1)2}(1-\mu^2\cosh^2\omega_z^{(0,1)})}, \tag{54}$$

$$f^{(j)}(x) = \frac{-4t''(x,\omega_y^{(0)})}{1-\mu^2} \cdot \frac{\sin\sigma_z^{(0,j)} - \sigma_z^{(0,j)}\cos\sigma_z^{(0,j)}}{2\sigma_z^{(0,j)3} - \sigma_z^{(0,j)2}\sin 2\sigma_z^{(0,j)}} =$$

$$= \frac{2t''\cos\sigma_z^{(0,j)}}{\sigma_z^{(0,j)2}(1-\mu^2\cos^2\sigma_z^{(0,j)})}, \; j = 2,3,4,\ldots. \tag{55}$$

We cannot use the same technique to evaluate $f^{(0)}$, because $dS^{(0)}/dz \equiv 0$. Instead we use (36) and compute $f^{(0)}$ once the other coefficients are known, i.e.

$$f^{(0)}(x) = f(x,\omega_y^{(0)},z) - \sum_{j=1}^{\infty} f^{(j)}(x,\omega_y^{(0)})S^{(j)}(\omega_y^{(0)},z).$$

This equation is valid for all values of z, but the choice $z = -1$ makes the occuring expressions particularly simple. By inserting Eqs. (54) and (55) we get

$$f^{(0)}(x) = -\frac{t(x,\omega_y^{(0)})}{1-\mu^2} - 2t''(x,\omega_y^{(0)})Q, \tag{56}$$

where

$$Q = \frac{\cosh\omega_z^{(0,1)}}{\omega_z^{(0,1)2}(1-\mu^2\cosh^2\omega_z^{(0,1)})} + \sum_{j=2}^{\infty} \frac{\cos\sigma_z^{(0,j)}}{\sigma_z^{(0,j)2}(1-\mu^2\cos^2\sigma_z^{(0,j)})}. \tag{57}$$

3 Analysis of the Iteration

In this section we prove convergence of the iteration for sufficiently small Froude numbers. The proof consists of estimates of the solutions to the two subproblems. In §3.1, we estimate the x– and y–derivatives of the solution to the definite problem at the surface in terms of the forcing h on the body. Thereafter, in §3.2, we derive estimates for the x–, y– and z–derivatives of the solution to the indefinite problem in terms of the forcing t along the surface. These estimates will be used to bound the normal derivative of the solution to the indefinite problem along the fictitious boundary of the body. In §3.3 we will combine the estimates for the definite and the indefinite subproblems to prove convergence of the iteration.

To begin with, we define some norms that we are going to use in the following:

$$
\begin{array}{ll}
|f|^2_{2,2,2} & = \int_{-1}^{0}\int_{-a}^{a}\int_{-\infty}^{\infty} \bar{f}\cdot f dxdydz, \\
|f|^2_{\infty,2,2} & = |\int_{-1}^{0}\int_{-a}^{a} \bar{f}\cdot f dydz|_{\infty,in\ x}, \\
|f|^2_{\infty,2} & = |\int_{-1}^{0} \bar{f}\cdot f dz|_{\infty,in\ x}, \\
|f|^2_{2,body} & = \oint_{body} \bar{f}\cdot f dS, \\
|f|^2_{2,2,s} & = \int_{-\infty}^{\infty}\int_{-a}^{a} \bar{f}(x,y,0)\cdot f(x,y,0) dxdy, \\
|f|^2_{\infty,2,s} & = |\int_{-a}^{a} \bar{f}(x,y,0)\cdot f(x,y,0) dy|_{\infty,in\ x}.
\end{array}
\tag{58}
$$

Henceforth, C will denote a generic constant which is independent of μ.

3.1 Estimate for the Definite Subproblem

It is well known, cf. [3], that x- and y-derivatives of ϕ^I along the surface can be estimated in terms of the forcing h. We make this statement more precise in

Lemma 1

$$
\left|\frac{\partial^{p+q}\phi^I}{\partial x^p \partial y^q}\right|_{2,2,s} \leq C_{p,q}\cdot L^2 |h|_{\infty,body},\ p=1,2,3,\ldots,\ q=0,1,2,\ldots,
$$

where $C_{p,q}$ are bounded constants and L is a typical lengthscale of the body.

In the domains ahead of and behind the body, the solution of the definite subproblem can be found by separation of variables. Let the body be contained in $-\beta \leq x \leq \beta$. Fourier expanding the solution in the y– and the z–direction yields,

$$
\phi^I(x,y,z) = \sum_{k=0}^{\infty}\sum_{j=0}^{\infty} p_{(k,j)} \exp(-\gamma^{(k,j)}|x|)\cdot\cos(\omega_z^{(k,j)}(1+z))\cdot\cos(\omega_y^{(k)}y), \tag{59}
$$

where $\gamma^{(k,j)2} = \omega_z^{(k,j)2} + \omega_y^{(k)2}$. The eigenvalues are given by $\omega_y^{(k)} = k\pi/2a$, $k = 0,1,2,\ldots$, $\omega_z^{(k,j)} = j\pi$, $j = 0,1,2,\ldots$. This equation is only valid for $|x| > \beta$. Hence, the forcing function $t(x)$ satisfies

$$
\begin{aligned}
t(x) &= \gamma^{(k,j)2}\sum_{k=0}^{\infty}\sum_{j=0}^{\infty} p_{(k,j)} \exp(-\gamma^{(k,j)}|x|)\cdot\cos(\omega_z^{(k,j)}(1+z))\cdot\cos(\omega_y^{(k)}y), \\
&\leq C\exp(\frac{-\pi}{2}|x|),
\end{aligned}
\tag{60}
$$

when $|x| > \beta$.

3.2 Estimates for the Indefinite Subproblem

The purpose of this section is to derive bounds for the maximum norm of the x, y and z–derivatives of ϕ^{II} in terms of the forcing t. To achieve these bounds we bound each Fourier mode separately and use Parseval's theorem. The continuous equation for each mode is given by (16-18). For each mode

respectively, this equation is splitted into one auxiliary (19) and one separable problem (21-22). To bound $\phi^{II} = \phi^a + \phi^s$ we bound ϕ^a and ϕ^s separately and add the bounds. In the case when $\omega_y^{(k)} = 0$, the problem simplifies to the 2D problem. In this paper we only bound the $k > 0$ modes and refer to the bounds in [7] for the mode $k = 0$.

Bounding the Fourier coefficients of ϕ^a: By inspection of (20) we have the following bounds for the solution to the auxiliary problem:

Lemma 2

$$|\phi^a|_{\infty,2} \leq \frac{|t|_{\infty,2}}{2 + \mu^2(\omega_y^{(k)2} - 2)}.$$

Bounding the separable problem: The separable problem is defined by (21-22). We estimate ϕ^s in five steps. First we bound the sum of the Fourier mode forcings $t(x, \omega_y^{(k)})$ in terms of $t(x, y)$ in L_2 norm. Then we bound the transformed forcing $v(x, \omega_y^{(k)})$ in terms of the forcing $t(x, \omega_y^{(k)})$ in maximum norm. We use Parseval's theorem to bound $\tilde{f}^{(j)}$. Third we estimate the solution of the transformed ODE's (40–42) in terms of the right hand sides $\tilde{f}^{(j)}$ in maximum norm. We can now again use Parseval's theorem to bound ϕ^s in terms of $t(x, \omega_y^{(k)})$ in maximum norm. Finally, we use Sobolev inequalities, Parseval's theorem and Lemma (2) to bound the solution to the indefinite subproblem $\phi^{II} = \phi^a + \phi^s$ in terms of $\mu^2 \phi^I_{xx}(x, y, 0)$ and its $x, y-$ derivatives in the L_2 norm.

Bounding the sum of Fourier coefficient Forcings: Parsevals theorem and (14) gives:

$$\sum_{k=0}^{\infty} |t(x, \omega_y^{(k)})|^2_\infty = |t(x, \cdot)|^2_{\infty,2,surf}, \tag{61}$$

Using the following Sobolev inequality, $|f|^2_\infty \leq \epsilon |f_x(\cdot)|^2_2 + C/\epsilon |f(\cdot)|^2_2$, we can easily bound the forcing to the separable problem, given by (19):

$$\sum_{k=0}^{\infty} |f(x, \omega_y^{(k)}, z)|^2_{\infty,2} = \frac{\sum_{k=0}^{\infty} |t_{xx} \cdot (1+z)^2 - \omega_y^{(k)2} t \cdot (1+z)^2 + 2t|^2_{\infty,2}}{(2 + \mu^2(\omega_y^{(k)2} - 2))^2} \leq$$

$$\leq \frac{C \cdot \left(|t|^2_{2,2,s} + |t_x|^2_{2,2,s} + |t_{xx}|^2_{2,2,s} + |t_{xxx}|^2_{2,2,s} + |t_{yy}|^2_{2,2,s} + |t_{yyx}|^2_{2,2,s} \right)}{(1-\mu^2)^2}. \tag{62}$$

Bounding $f^{(j)}$: First we bound $v(x, \omega_y^{(k)}, z)$ by inspection of (51,52)

$$|v|_{\infty,2} \leq C \cdot |f|_{\infty,2}. \tag{63}$$

Since the z–eigenfunctions, $\tilde{\zeta}^{(j)}$, $j = 1, 2, 3, \ldots$ of the transformed separable problem (37, 38) are orthogonal with respect to each other we can use Parsevals theorem to bound the sum of the transformed right hand sides, $\tilde{f}^{(j)}$:

$$\sum_{j=0}^{\infty} |\tilde{f}^{(j)}|_{\infty}^2 = |v|_{\infty,2}^2,\ j = 1, 2, 3 \ldots. \tag{64}$$

Bounding the solution to the transformed ODE's $\tilde{R^{(j)}}$: We begin by writing down the analytical solutions of the transformed correspondences to (40-42).

$$\tilde{R}^{(0)} = C_1 + C_2 x + \int_{-\infty}^{x} \int_{-\infty}^{\zeta} \tilde{f}^{(0)} d\xi d\zeta. \tag{65}$$

The upstream condition (3) implies that $C_1 = C_2 = 0$. Since $\tilde{f}^{(0)} = 0$ for $\omega_y^{(k)} \neq 0$, we then have $\tilde{R}^{(0)} = 0$. The general solution of the transformation of (41) is calculated by integration twice.

$$\begin{aligned} \tilde{R}^{(1)} = & C_3 \cos(\kappa^{(1)} x) + C_4 \cos(\kappa^{(1)} x) \\ & + \frac{1}{2\kappa^{(1)}} \int_{-\infty}^{x} \cos(\kappa^{(1)}(\zeta - x)) \tilde{f}^{(1)} d\zeta \\ & - \frac{1}{2\kappa^{(1)}} \int_{-\infty}^{x} \cos(\kappa^{(1)}(\zeta - x)) \tilde{f}^{(1)} d\zeta, \end{aligned} \tag{66}$$

here $\kappa^{(1)2} = \omega_z^{(k,1)2} - \omega_y^{(k)2}$. Again (3) yields $C_3 = C_4 = 0$. For the transformation of (42) the general solution can be expressed according to:

$$\begin{aligned} \tilde{R}^{(j)} = & C_5^{(j)} \exp(\lambda^{(j)} x) + C_6^{(j)} \exp(-\lambda^{(j)} x) \\ & - \frac{1}{2\lambda^{(j)}} \int_{-\infty}^{x} \exp(\lambda^{(j)}(\zeta - x)) \tilde{f}^{(j)} d\zeta \\ & - \frac{1}{2\lambda^{(j)}} \int_{x}^{\infty} \exp(-\lambda^{(j)}(\zeta - x)) \tilde{f}^{(j)} d\zeta, \end{aligned} \tag{67}$$

here $\lambda^{(j)2} = \sigma_z^{(k,j)2} + \omega_y^{(k)2}$ and $k = 1, 2, 3, \ldots,\ j = 2, 3, 4, \ldots$. By assuming the solution to be bounded at infinity we get $C_5^{(j)} = C_6^{(j)} = 0$.

The decay of $t(x)$, given by (60) implies that the forcing functions $\tilde{f}^{(j)}$ will satisfy:

$$|\tilde{f}^{(j)}(x)| \leq C \exp(-\frac{\pi}{2}|x|),\ j = 0, 1, 2, \ldots, \tag{68}$$

for $|x| > \beta$. We bound the solutions to the transformed ODE's, $(\tilde{R}^{(j)})$, by inspection of (65-67), respectively:

$$\begin{aligned} |\tilde{R}^{(0)}|_{\infty} &\leq CL\, |\tilde{f}^{(0)}|_{\infty}, \\ |\tilde{R}^{(1)}|_{\infty} &\leq CL\mu^2 |\tilde{f}^{(1)}|_{\infty}, \\ |\tilde{R}^{(j)}|_{\infty} &\leq \frac{CL}{\lambda^{(j)}} |\tilde{f}^{(j)}|_{\infty},\ j = 2, 3, 4, \ldots. \end{aligned} \tag{69}$$

Bounding $\phi^s(x,\omega_y^{(k)},z)$ by t: We can now use Parsevals theorem again and bound $\tilde{\phi}^s$ as the sum of $\tilde{R}^{(j)}$.

$$|\tilde{\phi}^s|^2_{\infty,2} = \sum_{j=0}^{\infty} |\tilde{R}^{(j)}|^2_{\infty}. \tag{70}$$

To obtain a bound for ϕ^s, we only need to bound the inverse transform (37,38), given by:

$$\phi^s = \alpha^{(k,0)} \cosh(\alpha^{(k,0)}\,\xi) \int_0^{\xi} \frac{\tilde{\phi}^s}{\cosh(\alpha^{(k,0)}\,\zeta)} d\zeta, \tag{71}$$

$$\phi^s = \beta^{(k,1)} \cos(\beta^{(k,1)}\,\xi) \int_0^{\xi} \frac{\tilde{\phi}^s}{\cos(\beta^{(k,1)}\,\zeta)} d\zeta, \tag{72}$$

by inspection of (71,72) we immediately get the bound:

$$|\phi^s|_{\infty,2} \leq C \cdot |\tilde{\phi}^s|_{\infty,2}. \tag{73}$$

Using (63,64,69,70) and (73) gives:

$$|\phi^s|_{\infty,2} \leq C \cdot L^2 |f|_{\infty,2} \leq C \cdot L^2 \frac{|t_{xx} \cdot (1+z)^2 - \omega_y^{(k)2} t \cdot (1+z)^2 + 2t|_{\infty,2}}{2 + \mu^2(\omega_y^{(k)2} - 2)}. \tag{74}$$

Bounding $\phi^{II} = \phi^a + \phi^s$, by using Lemma (2), gives:

$$|\phi^{II}|_{\infty,2} \leq C \cdot L^2(|t|^2_{\infty,2} + |t_{xx} \cdot (1+z)^2 - \omega_y^{(k)2} t \cdot (1+z)^2 + 2t|_{\infty,2}). \tag{75}$$

We use Parsevals theorem to bound $\phi^{II}(x,y,z)$:

$$|\phi^{II}|^2_{\infty,2,2} \leq \sum_{k=0}^{\infty} |\phi^{II}|^2_{\infty,2}. \tag{76}$$

Now, (62) gives:

Lemma 3

$$|\phi^{II}|_{\infty,2,2} \leq C \cdot L^2(|t|_{2,2,s} + |t_x|_{2,2,s} + |t_{xx}|_{2,2,s} + |t_{xxx}|_{2,2,s} + |t_{yy}|_{2,2,s} + |t_{yyx}|_{2,2,s}).$$

We use a Sobolev inequality to bound the maximum norm of $\phi^{(II)}$: in terms of the corresponding L-2 norm.

$$|\phi^{II}|_{\infty} \leq C(|\phi^{II}|_{\infty,2,2} + |\phi^{II}_y|_{\infty,2,2}). \tag{77}$$

To bound ϕ^{II}_n we use the relation $f_n = n \cdot \nabla f$:

$$|\phi^{II}_n|^2_{\infty} \leq |\phi^{II}_x|_{\infty} + |\phi^{II}_y|_{\infty} + |\phi^{II}_z|_{\infty}. \tag{78}$$

To bound ϕ_n^{II}, we need corresponding bounds to Lemma (3) for $\phi_x, \phi_{xy}, \phi_y, \phi_{yy}$, ϕ_z, ϕ_{zy} The z-derivatives are bounded by (9), which gives $|\phi_{zz}^{II}|_\infty \leq |\phi_{xx}^{II}|_\infty + |\phi_{yy}^{II}|_\infty$. We can therefore bound the aforementioned derivatives by using bounds for x- and y-derivatives of ϕ^{II}. We construct these bounds by differentiating the separable problem with respect to x, y etc., and use the same bounding technique as for ϕ^s above.

Using these bounds together with (77,78) and $t(x,y) = -\mu^2 \phi_{xx}^I(x,y,0)$ we have:

Lemma 4

$$|\phi_n^{II}|_{\infty,body}^2 \leq \mu^2 \sum_{p=2}^{7} \sum_{q=0}^{5} |\frac{\partial^{p+q}\phi^I}{\partial x^p \partial y^q}|_{2,surf}.$$

3.3 Proof of Convergence of the Iterative Cycle.

We denote the solution to subproblem 1, 2 resp. at iterate i: ϕ_i^I, ϕ_i^{II} and introduce:

$$\psi_i^I = \phi_{i+1}^I - \phi_i^I, \ \psi_i^{II} = \phi_{i+1}^{II} - \phi_i^{II}. \tag{79}$$

The problems for ψ^I and ψ^{II} are easily obtained by subtracting two successive subproblems for ϕ^I,ϕ^{II}, resp. Lemma (1) and (4) gives the following bounds for ψ^{II} and ψ^I.

$$|\psi_{i,n}^{II}|_{\infty,body} \leq C \cdot \mu^2 \cdot L^2 \sum_{p=2}^{7} \sum_{q=0}^{5} |\frac{\partial^{p+q}\psi_i^I}{\partial x^p \partial y^q}|_{2,2,surf}, \tag{80}$$

$$|\frac{\partial^{p+q}\psi_i^I}{\partial x^p \partial y^q}|_{2,2,surf} \leq C_{p,q} \cdot L^2 \cdot |\psi_{i-1,n}^{II}|_{\infty,body}, \ p = 0,1,2,\ldots, \ q = 0,1,2,.. \tag{81}$$

If we combine these bounds, we get.

Theorem 1

$$|\psi_{i,n}^{II}|_{\infty,body} \leq C\mu^2 L^4 |\psi_{i-1,n}^{II}|_{\infty,body}. \tag{82}$$

If we choose μ be sufficiently small, we have: $C\mu^2 L^4 < 1$. This proves convergence for the iteration.

4 Farfield Boundary Conditions

To carry out the practical calculation it is necessary to bound the computational domain and introduce artificial boundary conditions at the farfield boundaries. Here, we truncate the computational domain for the definite problem to $-b < x < b$, $-a < y < a$, where a, b are positive, see figure 2.

In this section, we present the inflow, outflow and the side wall boundary conditions. The effect of the in and outflow boundary conditions on the solution will be analysed for the definite subproblem in §4.1. In §6 we present numerical

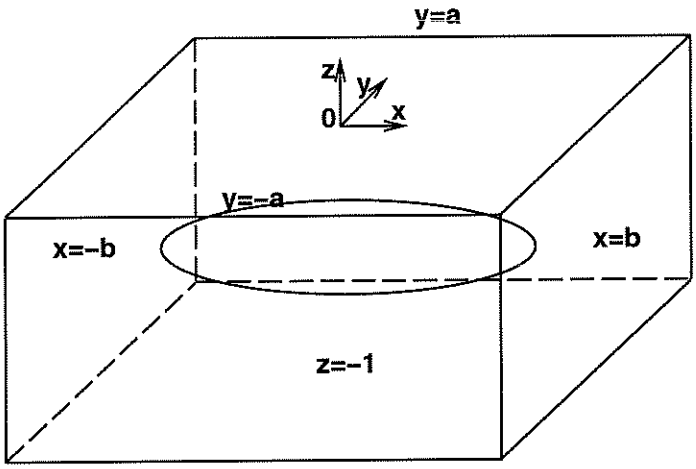

Figure 2: The computational domain is chosen to be a box surrounding the submerged body.

experiments to verify the analysis and that the influence of the approximate boundary conditions is small if the computational domain is made sufficiently large.

In order to solve the indefinite subproblem numerically, we must replace $t(x)$ by a smooth function $\tilde{t}(x) =: P(x)t(x)$ which has compact support in the computational domain. In addition, $P(x)$ must have two continuous derivatives, so that $\tilde{t}''$ is well defined. A cut-off function furnished with these properties is yielded by

$$P(x) = \begin{cases} 0, & -\infty < x \le -b, \\ p_1((-b+\epsilon-x)/\epsilon), & -b < x < -b+\epsilon, \\ 1, & -b+\epsilon \le x \le b-\epsilon, \\ p_1((-b+\epsilon+x)/\epsilon), & b-\epsilon < x < b, \\ 0, & b \le x < \infty, \end{cases} \tag{83}$$

where $\epsilon > 0$ and $p_1(\xi) = 1 - 10\xi^3 + 15\xi^4 - 6\xi^5$, this cutoff function is used for $-a \le y \le a$. We will denote the solution of (40–42) corresponding to the modified forcing by $\tilde{R}^{(k)}$. In the domains where $\tilde{t} = 0$, we can solve (40–42) analytically. These analytical solutions are used to form relations between the solution and its normal derivative which must be satisfied by any solution that is bounded at infinity and fulfills the radiation condition (12). These relations are used as farfield boundary conditions. They are given by

$$\tilde{R}^{(0)} = 0, \ \frac{d\tilde{R}^{(0)}}{dx} = 0, \ x = -b, \text{ if } \omega_y = 0, \tag{84}$$

$$\tilde{R}^{(1)} = 0, \ \frac{d\tilde{R}^{(1)}}{dx} = 0, \ x = -b, \tag{85}$$

$$\frac{d\tilde{R}^{(j)}}{dx} - \sqrt{\sigma_z^{(j)2} - \omega_y^2}\tilde{R}^{(j)} = 0, \ x = -b, \ j = 2, 3, \ldots, \tag{86}$$

$$\frac{d\tilde{R}^{(j)}}{dx} + \sqrt{\sigma_z^{(j)2} + \omega_y^2}\tilde{R}^{(j)} = 0,\ x = b,\ j = 2, 3, \ldots. \tag{87}$$

The boundary conditions (84–87) are exact. The difference between $R^{(j)}$ and $\tilde{R}^{(j)}$ therefore only depends on the difference between $t(x)$ and $\tilde{t}(x)$. A study of the behaviour of the solution ahead of and behind the body is given by N. A. Petersson, see [9].

We also have to introduce side-wall boundary conditions for the indefinite subproblem:

$$\phi_y^{II}(x, a, z) = 0,\ -\infty < x < \infty,\ -1 \le z \le 0, \tag{88}$$
$$\phi_y^{II}(x, -a, z) = 0,\ -\infty < x < \infty,\ -1 \le z \le 0. \tag{89}$$

For the definite subproblem, we enforce side–wall boundary conditions

$$\phi_y^{I}(x, a, z) = 0,\ -\infty < x < \infty,\ -1 \le z \le 0, \tag{90}$$
$$\phi_y^{I}(x, -a, z) = 0,\ -\infty < x < \infty,\ -1 \le z \le 0. \tag{91}$$

The boundary conditions (88–91) model the flow in a canal that is $2a$ wide. In §5, we study the effect of these bc's numerically by comparing computations made in canals of different widths.

Finally, we apply the following artificial inflow and outflow boundary conditions for the definite subproblem:

$$\phi^{I}(-b, y, z) = 0,\ -a \le y \le a,\ -1 \le z \le 0, \tag{92}$$
$$\phi_x^{I}(b, y, z) = 0,\ -a \le y \le a,\ -1 \le z \le 0. \tag{93}$$

These conditions are local, which makes an iterative solver easy to apply. In order to motivate that the effect of these artificial boundary conditions on the solution to the definite subproblem is small we study the behaviour of the solution ahead of and after the submerged body in §4.1. We there find that the solution of the definite subproblem is decaying exponentially ahead and outside the submerged body and that the first x- derivative of the solution is decaying exponentially after the body. Knowing this and using a simple scaling argument, cf. [8] one can easily show that the error in ϕ^I due to the inflow and outflow boundary conditions decays exponentially fast as a function of the minimum distance between the body and the in/outflow boundary. Analogously one shows that the error in ϕ^I due to the sidewise boundary conditions decreases exponentially fast as a function of the minimum distance between the body and the side boundary.

4.1 Behaviour of the Solution to the Definite Problem ahead of and after the Submerged Body.

We show that the solution to the definite subproblem decays exponentially ahead of and that the x-derivatives decays exponentially after the submerged body. We therefore consider the following halfspace problems, ahead we have:

$$\Delta\phi^I = 0,\ -\infty < x < -b,\ -a < y < a,\ -1 < z < 0, \tag{94}$$

together with the boundary conditions

$$\begin{array}{l} \phi^I_z = 0,\ -\infty < x < -b,\ -a < y < a,\ z = -1, 0, \\ \phi^I = f_1,\ x = -b,\ -a < y < a,\ -1 < z < 0, \end{array} \tag{95}$$

and after:

$$\Delta\phi^I = 0,\ b < x < \infty,\ -a < y < a,\ -1 < z < 0, \tag{96}$$

having the boundary conditions

$$\begin{array}{l} \phi^I_z = 0,\ b < x < \infty,\ -a < y < a,\ z = -1, 0, \\ \phi^I = f_2,\ x = b,\ -a < y < a,\ -1 < z < 0, \end{array} \tag{97}$$

we assume that f_1 and f_2 are bounded by the constant C_2, the side-wall bc's are given by (90,91). We also require the solution to be bounded when $x \to \pm\infty$. To solve this problem we separate variables using the ansatz: $\phi^I(x, y, z) = \Phi^I(x, z) \cdot Y(y)$, this gives the following equation for $Y(y)$:

$$Y'' + \omega_y^{(k)2} \cdot Y = 0,\ -a < y < a, \tag{98}$$

the solution to this equation is given by:

$$Y(y) = \cos(\omega_y^{(k)}(y + a)), \tag{99}$$

the BC's (95,97) gives that $\omega_y^{(k)} = k\pi/2a,\ k = 0, 1, 2, \ldots$. The equation for Φ^I is:

$$\Phi^I_{xx} - \omega_y^{(k)2}\Phi^I + \Phi^I_{zz} = 0,\ x < -b,\ x > b,\ -1 < z < 0. \tag{100}$$

We separate variables again by entering the ansatz: $\Phi^I(x, z) = X(x) \cdot Z(z)$, this gives:

$$Z_{zz} + \omega_z^{(k,j)2} Z = 0,\ -1 < z < 0, \tag{101}$$

the solution to this equation is given by:

$$Z(z) = \cos(\omega_z^{(k,j)}(1 + z)), \tag{102}$$

where $\omega_z^{(k,j)} = j\pi/1,\ j = 0, 1, 2, \ldots$. We can now express Φ^I as:

$$\Phi^I(x, \omega_y^{(k)}, \omega_z^{(k,j)}) = \sum_{j=0}^{\infty} X^{(k,j)}(x) \cdot \cos(\omega_z^{(k,j)}(1 + z)). \tag{103}$$

The equation for $X(x)$ is:

$$X_{xx} - \alpha^{(k,j)2} X = 0,\ x < -b,\ x > b, \tag{104}$$

where $\alpha^{(k,j)2} = \omega_y^{(k)2} + \omega_z^{(k,j)2}$ is positive and real. The eigenfunctions in the x-direction are:

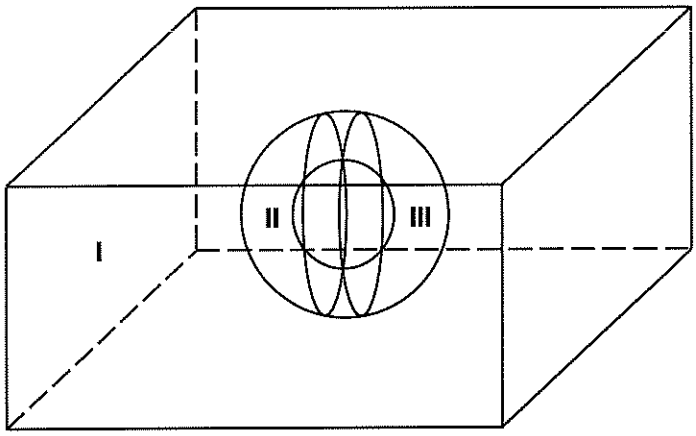

Figure 3: The overlapping domains covering a sphere in a box. Domain II and III cover roughly half of the sphere each. Domain I is covering the outer parts of the box.

$$\begin{aligned} X^{(0)}(x) &= A_0 + B_0 x, \\ X^{(k)}(x) &= A_k \exp(\alpha^{(k,j)} x) + B_k \exp(-\alpha^{(k,j)} x). \end{aligned} \tag{105}$$

To make Φ^I bounded when $|x| \to \infty$ we must have that:

$$\begin{aligned} A_0 &= 0, \text{ is set to fix the solution,} \\ A_k &= 0, \text{ after the body, } k = 1, 2, 3, \ldots, \\ B_k &= 0, \text{ ahead of the body, } k = 0, 1, 2, \ldots. \end{aligned} \tag{106}$$

The solution to the definite subproblem is therefore decaying exponentially before the submerged body and the first x-derivative of the solution is decaying exponentially after the submerged body.

5 Numerical Method

In this section we describe the numerical method developed in this paper. We elaborate on how we solve the definite subproblem in §5.1 and in §5.2 we comment on the numerical method for the indefinite subproblem.

5.1 Solving the Definite Subproblem

We discretize the definite subproblem by second order accurate finite differences using a composite overlapping grid. To apply this technique, we divide the domain into simple overlapping subdomains and cover each subdomain with a component grid, see figure 3.

The subdomains attaching to the body are covered with bodyfitted curvilinear grids and the surrounding sea is covered with one or several Cartesian grids. The main advantage with this method compared to discretizing the whole domain with one single grid is that each component grid can be made logically

rectangular and without singularities. The component grids can be constructed almost independently of each other. The restrictions are that the component grids need to overlap each other sufficiently where they meet and the union of the component grids have to cover the whole computational domain. The gridfunctions on the component grids are coupled by continuity requirements, which are enforced by applying sufficiently accurate, in this case tri–quadratic, interpolation relations between the gridfunctions at the interiour boundaries where the component grids overlap. A comprehensive description of this approach for a related problem is given in [10].

We use the fortran software package CMPGRD to construct the composite grids. Many aspects of composite grids and how to use this package are described in [1], [6] and [2]. An example of a composite overlapping grid used to discretize the domain around a sphere is found in figures 5–fig:sph2

The resulting linear system of equations is solved with the BCG method, using the CGES solver, see [5]. This method requires of the order $\mathcal{O}(n^{4/3})$ operations where n equals the number of used gridpoints in the composite grid.

5.2 Solving the Indefinite Subproblem

Instead of continuous Fourier transform in the y-coordinate (13), we use a discrete FFT, from the Slatec package. The expansion in the z-coordinate is calculated exactly as described in §2. The product of the number of terms in the series expansions of ϕ^{II} in y and z (35), which equals the number of ordinary differential equations (40–42) that must be solved, has to be limited to improve the efficiency of the numerical calculation. We found by numerical experiments that it was sufficient to retain the ten first terms in the z-eigenfunction expansion. This is related to the fact that the solution is smooth. The remaining terms were found to have neglible effect on the solution.

We approximate the ordinary differential equations (40–42) by second order accurate central differences. The character of the solution to the definite problem is smooth and local, whereas the solution to the indefinite problem contains downstream waves with a relatively small wavelength. Therefore, we utilize a Cartesian grid with finer gridstep that covers a larger x-interval to compute the solution of the indefinite subproblem. The resulting tridiagonal systems of equations are solved by the subroutine DNBSL in the SLATEC package. The work needed to obtain a solution to the indefinite subproblem is of the order $\mathcal{O}(n_1)$, where n_1 is the product of the number of gridpoints in the discretization of one ordinary differential equation and the number of terms we retain in the series expansion. With ten terms in the z - eigenfunction expansion, this n_1 is of the same order as the number of unknowns in the definite subproblem.

6 Numerical Results

In this section we present numerical results for a second order accurate discretization of (1–3). We study a number of test cases in §6.1. First we present an accuracy test which verifies that our implementation of the iterative method described in this paper is second order accurate. We verify numerically that

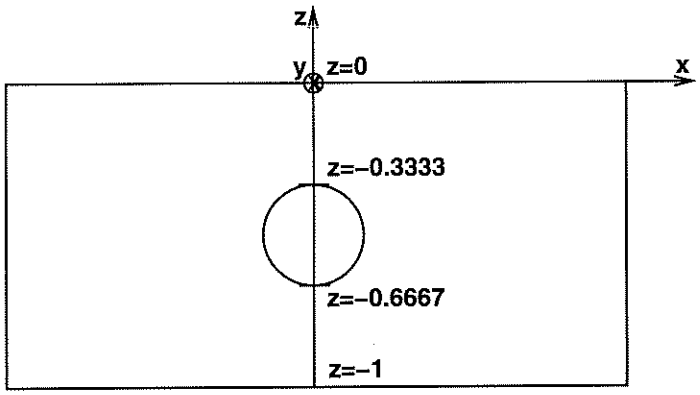

Figure 4: The test geometry, a sphere with radius 1/6. The center of the sphere is submerged 1/2.

the iterative method converges rapidly, and that the convergence rate improves when the Froude number decreases. We show that the convergence rate is essentially independent of the grid size. It is demonstrated that the iterative method is efficient from a computational point of view. In addition, we show that the error committed by truncating the domain and introducing farfield boundary conditions decays exponentially with the size of the computational domain.

6.1 Numerical Testing and Validation

To validate the iterative method we have studied a number of test cases. As a test body, we used a sphere with radius 1/6. The center of the sphere was submerged 0.5 below the free surface and located at $(x, y, z) = (0, 0, -0.5)$, see figure 4. The Froude number for these computations is: $\mu = 0.4$ unless otherwise specified. A composite grid that discretizes the submerged sphere and the surrounding liquid is displayed in figures 5–6. The composite grid consists of three component grids. two curvilinear grids that resolve the geometry of the sphere and one Cartesian grid that covers the outer flow domain.

To check the implementation of the iterative method and see that the discretization error is second order accurate, we compare the computed discrete solution for three different gridsteps $3h, 2h$ and h in table 1, the values are normalized by $|\phi_h|_\infty, |\phi_h|_{RMS}$. We clearly see that the solution is second order accurate. (RMS here denotes the usual root-mean-square norm ie. the discrete L_2 norm)

We show the convergence of the iterative method for Froude numbers 0.15–0.7 in table 2, where we plot the number of iterations needed to decrease the relative increment in each iteration to $1.E-05$. In the right column, we plot the number of iterations needed for convergence, when restarting from a solution for the next lower Froude number. From these results it is observed that the convergence of the iterative method is fast and that the number of iterations decreases when $\mu \to 0$, the latter result is clearly motivated by Theorem 1.

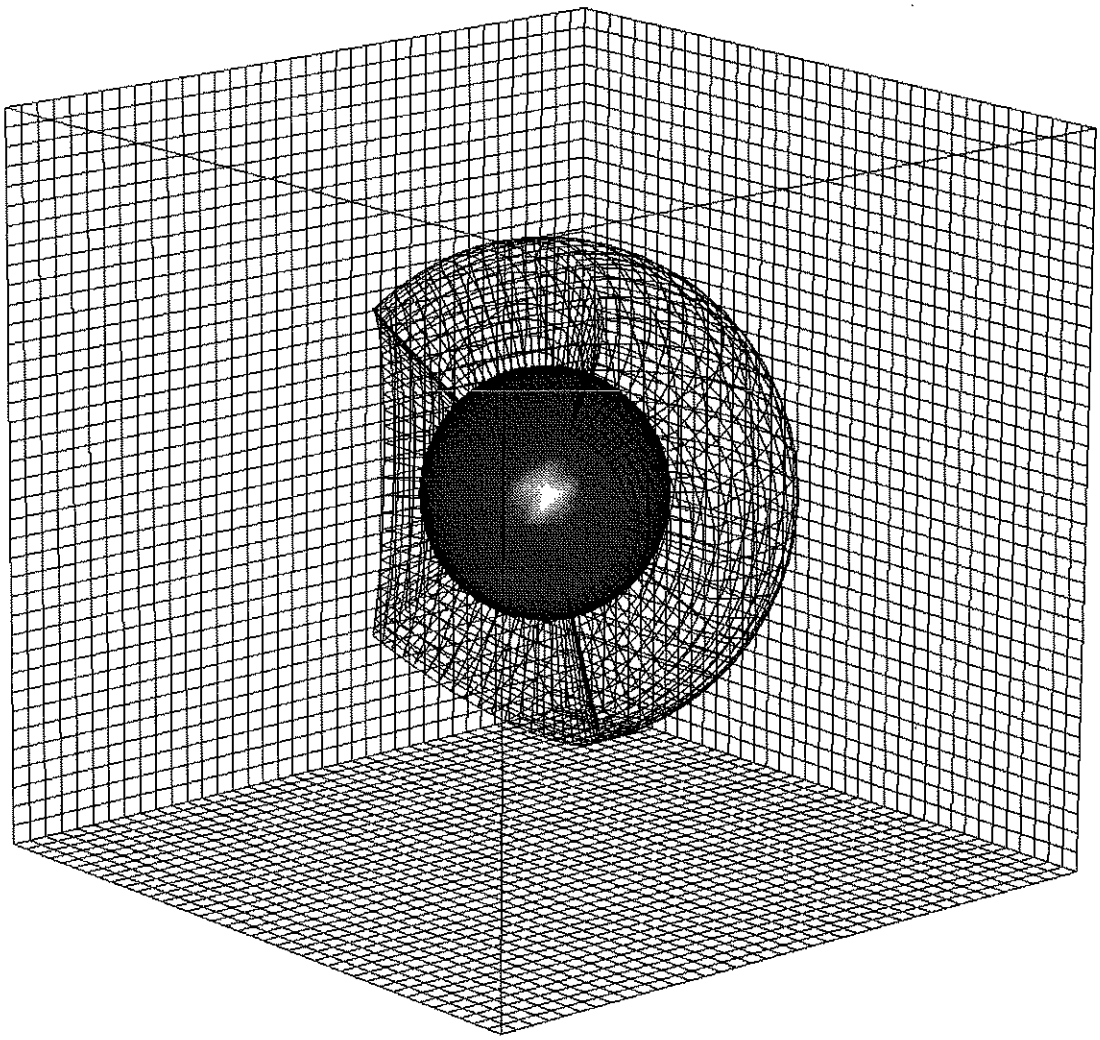

Figure 5: A composite overlapping grid discretizing a sphere in a box. The figure shows one of the curvilinear body attached component grids and the Cartesian box grid, also see the following figure.

	Absolute Norm	RMS Norm
$\phi_{3h} - \phi_h$	1.3E-01	1.7E-02
$\phi_{2h} - \phi_h$	4.9E-02	6.5E-03
conv. rate	2.0	2.0

Table 1: Accuracy test, we compare the solutions from grids with gridsteps, $h, 2h, 3h$. The differences are normalized by $|\phi_h|_\infty$. The convergence rate p, is defined by h^p.

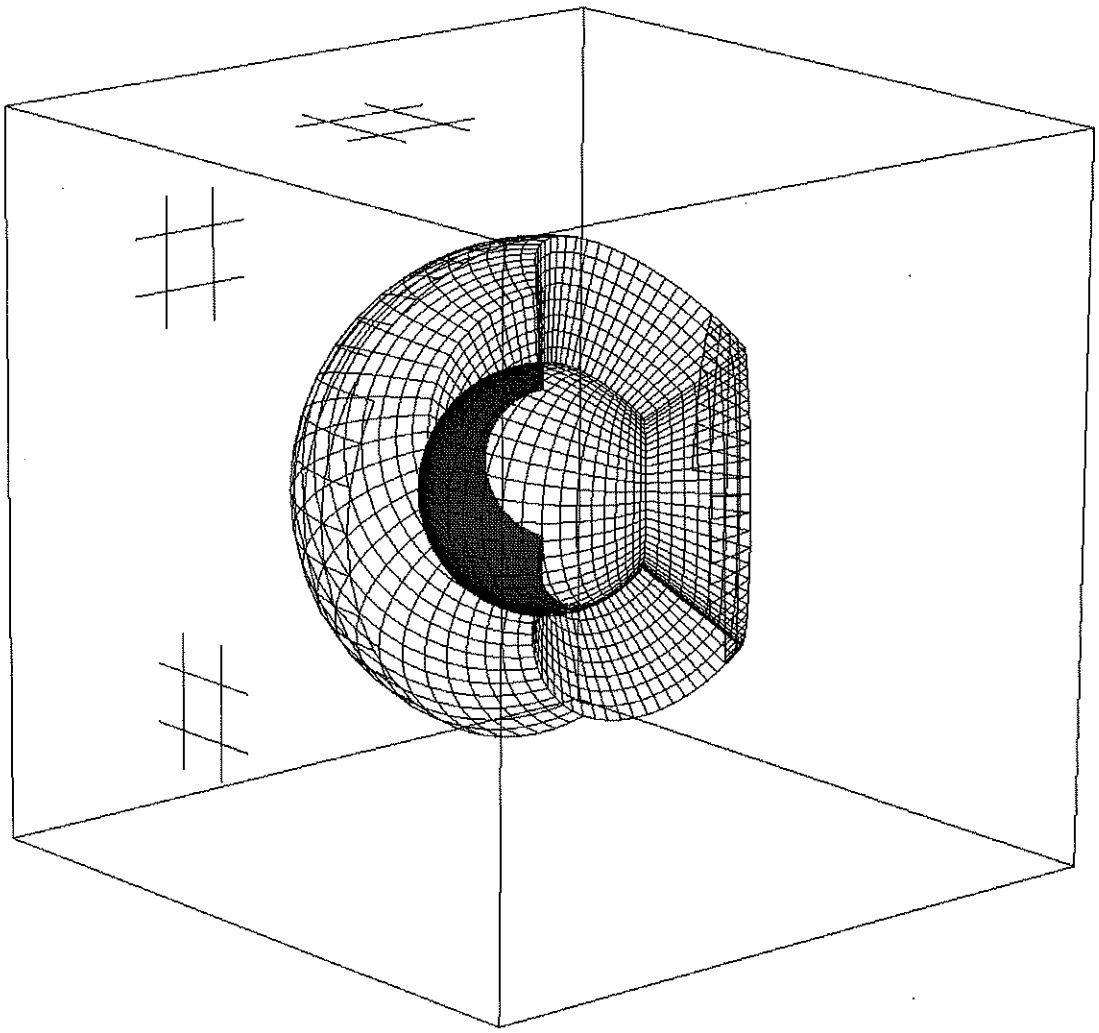

Figure 6: A composite overlapping grid discretizing a sphere in a box. The figure shows the other curvilinear body attached component grid, see the previous figure.

Froude number (μ)	nr. of iterations	restart
0.15	4	
0.20	5	3
0.25	6	4
0.30	6	4
0.35	7	4
0.40	8	4
0.45	9	5
0.50	11	6
0.55	14	7
0.60	23	10
0.65	34	20
0.7	div	div

Table 2: Nr. of iterations needed for convergence for Froude numbers, (μ), 0.15–0.70. In the right column, we plot the number of iterations needed for convergence, when restarting from a solution for the next lower Froude number.

gridstep	nr. of iterations
$2\sqrt{2}h$	7
$2h$	7
$\sqrt{2}h$	8
h	9

Table 3: Number of iterations for convergence using different gridsteps. The convergence rate is weakly dependent of the gridstepsize.

In table 3 we show the number of iterations needed to decrease the relative increment in each step of the iteration to $1.E-05$ for the gridsteps $h-2\sqrt{2}h$. We see that the convergence rate is only weakly dependent of the gridsize.

Furthermore, in figure 7 we show the max-norm of the relative increment at each iteration. We clearly see, which Theorem 1 suggests, that the convergence is exponential and fast.

We present the computed free surface above the submerged sphere in figure 8 where $\mu = 0.4$

To ensure that the iterative method gives the same solution as other methods, we compare the coefficient of drag (C_D) with computations made by Havelock [4], 1931, in table 4 where he computes the flow around a submerged sphere. The coefficient of drag is defined by:

$$C_D = \oint_{\text{body}} (2\phi_x + \phi_x^2 + \phi_y^2 + \phi_z^2)\, dS.$$

We have computed this integral by simply summing the contribution from every used gridpoint at the surface of the body multiplied with the surface

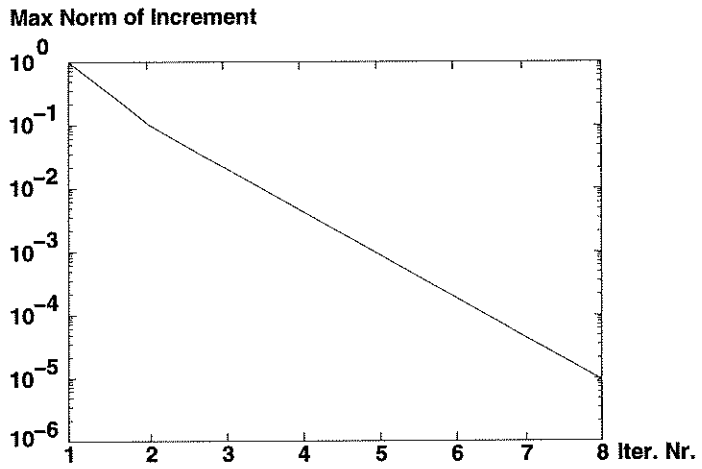

Figure 7: Increment of the solution at each iteration ($\mu = 0.4$). The increment is scaled with the previous solution.

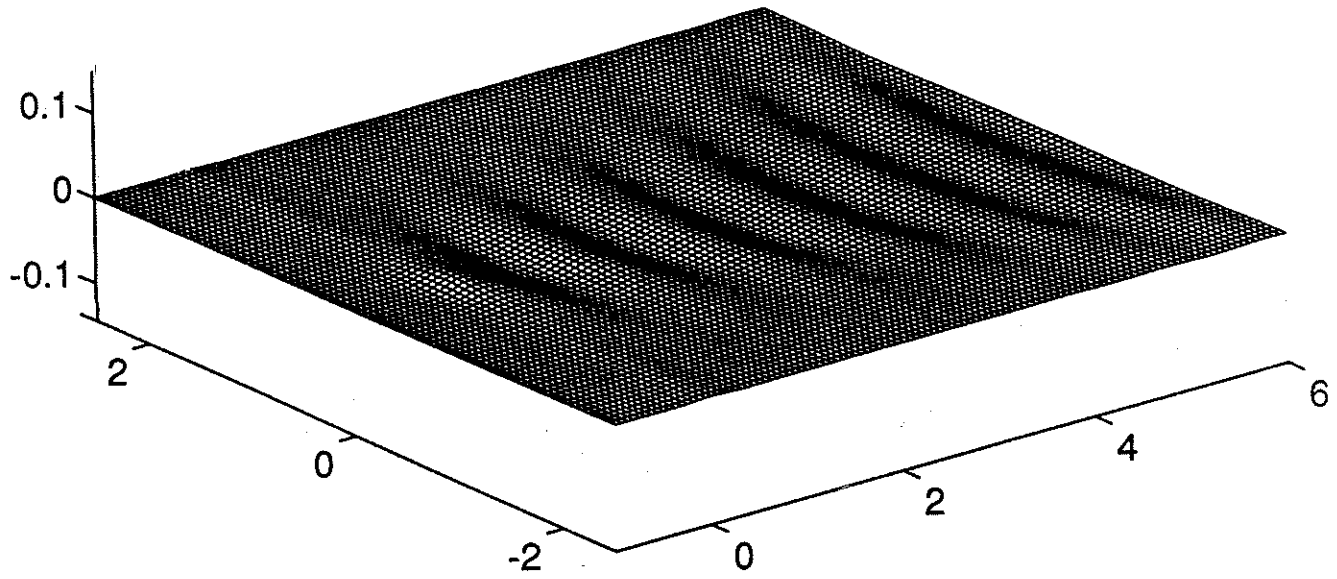

Figure 8: The surface above a sphere with $r = 0.1$ centered at $(0., 0., -0.5)$

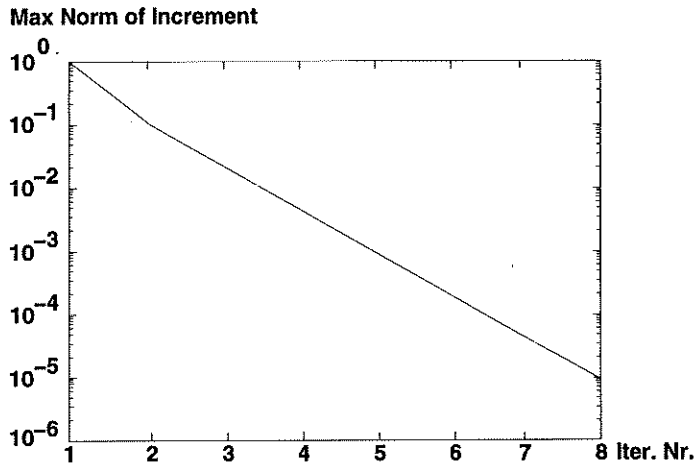

Figure 7: Increment of the solution at each iteration ($\mu = 0.4$). The increment is scaled with the previous solution.

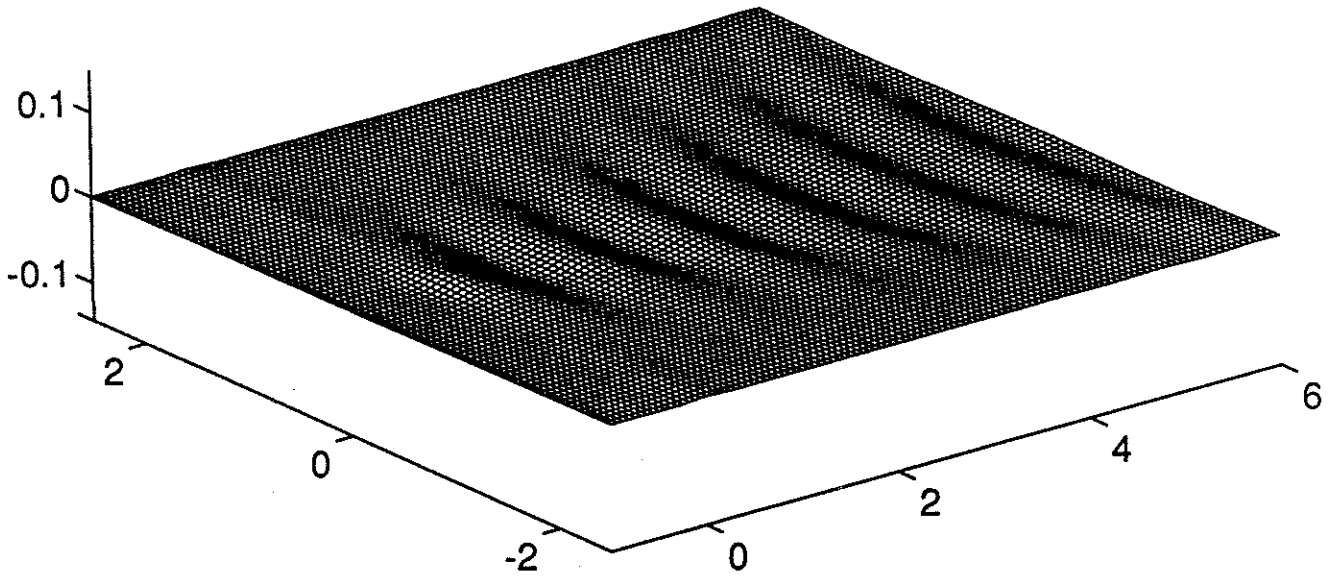

Figure 8: The surface above a sphere with $r = 0.1$ centered at $(0., 0., -0.5)$

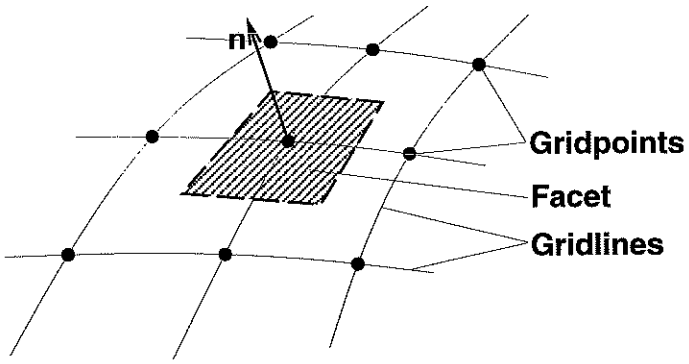

Figure 9: The body-surface facet, used for the integration of the coefficient of drag, C_D.

Froude Number (μ)	C_D Havelock	C_D present
0.40	3.5E-02	3.2E-02
0.45	4.8E-02	4.5E-02
0.50	5.8E-02	5.7E-02

Table 4: Comparison of coefficient of drag (C_D). In the left column we present Havelock's results and in the right column we display results from the present method. We find that there is good agreement between the results obtained by the two methods.

defined by figure 9. We see that there is good agreement with the previously computed C_D's.

To study the effect of the approximate inflow and outflow boundary conditions for the definite subproblem we compare the solutions for computational domains of different length in table 5. This indicates that the effect of the inflow and outflow boundary conditions decay exponentially with the minimum distance between the in- or outflow boundary and the submerged body.

To study the effect of the side-wise boundary conditions for the subproblems we compare the solutions for computational domains of different width in table 6. This result indicates that the effect of the side-wise boundary conditions

	Absolute Norm	RMS Norm
$\phi_{3l} - \phi_l$	8.9E-04	1.4E-04
$\phi_{3l} - \phi_{2l}$	7.6E-05	1.2E-05
ϕ_{3l}	2.7E-03	4.2E-04

Table 5: Comparison between solutions obtained by using grids of the different length's, $l, 2l, 3l$. The solutions are compared on the shortest domain. We observe that the difference decays exponentially with the length. This is confirmed by the theoretical predictions.

	Absolute Norm	RMS Norm
$\phi_{5w} - \phi_w$	4.5E-03	8.1E-04
$\phi_{5w} - \phi_{3w}$	3.7E-04	6.7E-05
ϕ_5	3.5E-03	6.4E-04

Table 6: Comparison between solutions obtained by using grids of the different width's, $w, 3w, 5w$. We observe that the difference decays exponentially with the width.

decay exponentially with the minimum distance between the boundary and the submerged body

7 Conclusions

In this paper we have developed and implemented an efficient Schwarz type iterative method for computing the steady linearized 3-D free surface potential flow around a submerged body. We construct the iterative method by decomposing the original problem into two simpler subproblems. The solution to the original problem is then calculated by an iteration between the subproblems.

The subproblems are chosen so that they are mathematically simple and computationally fast to solve. We prove that the iteration converges for sufficiently small Froude numbers. By numerical experiments, we have verified that the iterative method converges for realistic Froude numbers. The implementation of the present method is carefully validated - the numerical solution is found to be second order accurate. The work needed to solve a problem is found to be proportional to $n^{4/3}$, where n is the number of unknowns in the discretized problem. We have also compared the coefficient of drag with results obtained by existing methods and found good agreement.

The method can be extended to solve the corresponding potential problem with a nonlinear free surface boundary condition. It is furthermore straightforward to incorporate rotational and viscous effects in the method. This method could also be used to solve the potential flow in one subdomain, it could then be coupled to a method that computes the solution of a viscous rotational flow in another subdomain.

Acknowledgement

Prof. H. O. Kreiss is gratefully acknowledged for many fruitful discussions on the present problem. Furthermore he arranged a visit at UCLA for the author during the spring of -92.

The author is also indebted to *Dr. N. A. Petersson* who developed parts of the theory that this paper is based on, furthermore he contributed many valuable suggestions.

Dr. D. L. Brown is acknowledged for providing computer resources at Center for NonLinear Studies, LANL. Furthermore he arranged a visit at LANL for

the author during the fall of -92.

The author also wants to acknowledge *Dr's. G. Chesshire* and *W. D. Henshaw* for sharing their expertise on composite grids.

References

[1] D. L. Brown, G. Chesshire, and W. D. Henshaw. Getting started with CMPGRD, introductory user's guide and reference manual. report LA-UR-90-3729, Los Alamos National Laboratory, 1989.

[2] G. Chesshire and W. D. Henshaw. Composite overlapping meshes for the solution of partial differential equations. *JCP*, 90(1):1–64, 1990.

[3] R. Courant and D. Hilbert. *Methods of Mathematical Physics, vol II.* Interscience Publishers, 1962.

[4] T. H. Havelock. *The Collected papers of Sir T. H. Havelock on Hydrodynamics. The Wave Resistance of a Spheroid.* ONR, 1963.

[5] W. D. Henshaw. CGES user guide, version 1.00, a solver for steady state boundary value problems on overlapping grids. IBM Research Report RC 19361, IBM Research Division, Yorktown Heights, NY, 1994.

[6] W. D. Henshaw, G. Chesshire, and M.E. Henderson. On constructing three dimensional overlapping grids with CMPGRD. IBM research report, IBM Research Division, Yorktown Heights, NY, 1992.

[7] J. F. Malmliden. An efficient numerical method for 3d flow around a submerged body. Technical Report TRITA-NA-9306 (Submitted to Math. Comp.), Dep. of Numerical Analysis and Computing Science, Royal Inst. of Tech., 1993.

[8] J. F. Malmliden and N. A. Petersson. A fast iterative method to compute the flow around a submerged body. Technical Report LA-UR-93-0839, (to appear in Math. Comput.), Center for NonLinear Studies, Los Alamos National Laboratory, 1993.

[9] N. A. Petersson. A radiation boundary condition for linear 3-d steady ship waves. *Preprint*, 1990.

[10] N. A. Petersson and J. F. Malmliden. Computing the flow around a submerged body using composite grids. *J. Comput. Physics*, 105(1):47–57, 1993.

[11] G. B. Whitham. *Linear and nonlinear waves.* Wiley-Interscience, 1974.